# Neuroprotection of the Inner Retina Also Prevents Secondary Outer Retinal Pathology in a Mouse Model of Glaucoma

Sandeep Kumar, Hariharasubramanian Ramakrishnan, Suresh Viswanathan, Abram Akopian, and Stewart A. Bloomfield

Department of Biological and Vision Sciences, State University of New York College of Optometry, New York, New York, United States

Correspondence: Stewart A. Bloomfield, Department of Biological and Vision Sciences, State University of New York College of Optometry, 33 West 42nd Street, New York, NY 10036, USA; sbloomfield@sunyopt.edu.

**Received:** February 27, 2021
**Accepted:** June 24, 2021
**Published:** July 23, 2021

Citation: Kumar S, Ramakrishnan H, Viswanathan S, Akopian A, Bloomfield SA. Neuroprotection of the inner retina also prevents secondary outer retinal pathology in a mouse model of glaucoma. *Invest Ophthalmol Vis Sci.* 2021;62(9):35. https://doi.org/10.1167/iovs.62.9.35

**Purpose.** We examined structural and functional changes in the outer retina of a mouse model of glaucoma. We examined whether these changes are a secondary consequence of damage in the inner retina and whether neuroprotection of the inner retina also prevents outer retinal changes.

**Methods.** We used an established microbead occlusion model of glaucoma whereby intraocular pressure (IOP) was elevated. Specific antibodies were used to label rod and cone bipolar cells (BCs), horizontal cells (HCs), and retinal ganglion cells (RGCs), as well as synaptic components in control and glaucomatous eyes, to assess structural damage and cell loss. ERG recordings were made to assess outer retina function.

**Results.** We found structural and functional damage of BCs, including significant cell loss and dendritic/axonal remodeling of HCs, following IOP elevation. The first significant loss of both BCs occurred at 4 to 5 weeks after microbead injection. However, early changes in the dendritic structure of RGCs were observed at 3 weeks, but significant changes in the rod BC axon terminal structure were not seen until 4 weeks. We found that protection of inner retinal neurons in glaucomatous eyes by pharmacological blockade of gap junctions or genetic ablation of connexin 36 largely prevented outer retinal damage.

**Conclusions.** Together, our results indicate that outer retinal impairments in glaucoma are a secondary sequalae of primary damage in the inner retina. The finding that neuroprotection of the inner retina can also prevent outer retinal damage has important implications with regard to the targets for effective neuroprotective therapy.

Keywords: glaucoma, bipolar cells, horizontal cells, neuroprotection, retinal ganglion cells

Glaucoma is a neurodegenerative disease often associated with elevated intraocular pressure (IOP), which results in progressive degeneration of retinal ganglion cells (RGCs) and visual field deficits.[1,2] Although RGCs are the primary degenerative targets in glaucoma, the extent to which distal neurons are affected remains controversial. Some studies have found no evidence of outer retinal abnormalities,[3–6] but others have reported both structural and functional changes in cone photoreceptors,[7–11] bipolar cells (BCs),[12–17] and horizontal cells (HCs)[16,18] in both glaucoma patients and experimental animal models of glaucoma. Many parameters subserved by BCs and HCs are altered in glaucoma, consistent with functional deficits in outer retina.[19–24]

Structural changes localized to the outer retina are temporally correlated with inner retinal pathology in glaucoma patients and therefore appear dependent on the state of disease progression.[8,25] However, it is unclear whether these abnormalities result directly from glaucomatous insult or are a secondary consequence of inner retina damage. Like other neurodegenerative central nervous system diseases, glaucoma often follows a course of initial cell death due to the primary insult followed by a progressive secondary loss.[26,27] Thus, understanding the extent and timing of outer retina dysfunction is necessary to construct a more complete picture of glaucoma pathophysiology necessary to define targets for neuroprotective therapies.

Here, we examine outer retinal changes in a mouse microbead occlusion model of glaucoma. We found that the structure and function of BCs, as well as the dendritic/axonal organization of HCs, show substantial damage following induction of elevated IOP. Importantly, we observed that early structural changes to RGC dendrites precede those to BC axon terminals in the inner plexiform layer (IPL). Finally, we found that protection of inner retinal neurons in glaucomatous eyes by the previously reported blockade of gap junctions (GJs)[28] significantly reduces abnormalities in the outer retina. These results indicate that outer retinal impairments in glaucoma are a secondary sequalae of primary damage in the inner retina, a finding that contributes






Investigative Ophthalmology & Visual Science

to identifying potential targets for effective neuroprotective therapy.

## Methods

### Experimental Animals

Experiments were performed on C57BL/6 wild-type (WT) mice and on connexin36 knock-out ($Cx36^{-/-}$) mice and their wild-type ($Cx36^{+/+}$) littermates, 3 to 4 months old and of either sex. The $Cx36^{-/-}$ and $Cx36^{+/+}$ mice were derived from F2 C57BL/6-129SvEv mixed-background litters.[29] All animal procedures were in compliance with the National Institutes of Health Guide for the Care and Use of Laboratory Animals and the ARVO Statement for the Use of Animals in Ophthalmic and Vision Research, and they were approved by the institutional animal care and use committee at the State University of New York College of Optometry.

### Induction of Elevated IOP

IOP was elevated by unilateral injection of polystyrene microbeads (Invitrogen, Carlsbad, CA, USA), 10 µm in diameter, into the anterior chamber.[28,30] An equivalent volume of PBS was injected into contralateral eyes to provide control (sham) measurements. A second microbead injection was performed at week 4, which maintained elevated IOP for at least 8 weeks. All injections were performed on animals anesthetized with a ketamine/xylazine mixture and topical application of proparacaine. IOP measurements were performed weekly between 10 AM and 12 PM, to minimize effects of diurnal IOP variation. Six measurements were obtained per eye and averaged.

### Blockade of Gap Junctions

The GJ blocker meclofenamic acid (MFA, 20 mg/kg/day; Sigma-Aldrich, St. Louis, MO, USA) was administered via subcutaneous osmotic minipumps (ALZET 2004; DURECT, Cupertino, CA), as described previously.[28] Mice were anesthetized under isoflurane anesthesia, and pumps were implanted 1 day prior to microbead injection and replaced at 4 weeks.

### Immunohistochemistry

The immunohistochemical methods have been described previously.[28,31,32] Eyecups were fixed with 4% paraformaldehyde, cryoprotected, and embedded in tissue freezing medium (Electron Microscopy Sciences, Hatfield, PA, USA), and 10- to 15-µm-thick frozen sections were cut. The tissues were incubated with diluted primary antibodies overnight (sections) or for 48 hours (whole mounts), washed, and then incubated in secondary antibodies for 2 to 4 hours. Images of immunolabeled retinal sections or whole mounts from control and experimental groups were obtained with an Olympus FV1200 MPE confocal microscope (Olympus, Tokyo, Japan) using a 40× oil-immersion objective. High-resolution (1024 × 1024 pixels) *z*-stack images were taken using step sizes of 0.7 to 2.0 µm and compiled. The brightness and contrast of micrographs were adjusted using Photoshop CS6 (Adobe, San Jose, CA, USA). The primary antibodies were anti-PKCα (1:10,000; Sigma-Aldrich); anti-Chx10 (1:500; Santa Cruz Biotechnology, Dallas, TX, USA); anti-calbindin (1:500; Santa Cruz Biotechnology); anti-SMI32 (1:2000; Covance, Princeton, NJ, USA); anti-VGlut1 (1:150; BioLegend, San Diego, CA, USA); and anti-CtBP2 (1:500, Santa Cruz Biotechnology). Secondary antibodies were conjugated with Alexa Fluor 488, 594, and 633 (1:200; Thermo Fisher Scientific, Waltham, MA, USA).

### Assessment of Morphological Changes

Cell counts were made per lateral unit length of 300 µm in vertical sections, 10 to 15 µm thick. Measurements were made from the mid-periphery, 1.5 to 2.0 mm from the optic nerve head, within all four retinal quadrants (15–20 sections) and averaged, using at least three retinas for each condition. For measures of SMI32 labeling in flatmount retinas, three or four square areas (300 × 300 µm) in each quadrant in the mid-periphery were analyzed and averaged across four retinas each for control and experimental protocols. ImageJ software (National Institutes of Health, Bethesda, MD, USA) was used to quantify the number of pixels with immunolabels above background. The number of pixels positive for a marker was then divided by the total pixel number and presented as a percentage of covered area. This parameter was independent of differences in the intensity of label within or across retinas, as the analysis was performed with grayscale thresholding. All data were imported into SigmaPlot software (Systat Software, San Jose, CA, USA), and histograms were constructed.

### Electroretinogram Recording

The scotopic ERG responses were recorded from both eyes simultaneously. Visual stimuli consisted of brief (<5 ms) white Ganzfeld flashes ranging between –6.7 and 2.0 log scot cd·s/m$^2$, produced by an array of light-emitting diodes (Diagnosys, Lowell, MA). Responses were averaged over 40 to 50 trials for weak stimuli and fewer trials for stronger stimuli. Signals were amplified, filtered (1–300 Hz), and digitized at 1 kHz with a resolution of 0.1 µV.

### Statistical Analysis

Data are presented as mean ± SEM. Sample sizes (retinas, eyes, mice) were determined on the basis of our previous studies.[28,32] Sample sizes were determined using values of groups and common standard deviation. Calculations were performed using two-sided tests with alpha = 0.05 and power = 0.8. Samples were allocated to experimental groups according to genotype; therefore, there was no randomization. To compare two experimental groups, we used a two-tailed Student's *t*-test. Comparisons between larger groups were analyzed using one-way analysis of variance followed by Tukey's multiple comparison test. Values of $P < 0.05$ were considered statistically significant.

## Results

### Changes in Bipolar Cell Structure and Function in Glaucomatous Eyes

Unilateral injections of microbeads made at weeks 0 and 4 resulted in a sustained elevation of IOP from ~12 to 20 mm Hg for the entire 8-week period ($P < 0.001$ for all time points; $n = 10$ eyes/group) (Fig. 1A). We detected no sex-specific differences in mean IOP elevation. To study the effect of elevated IOP on outer retina function, we recorded

Investigative Ophthalmology & Visual Science

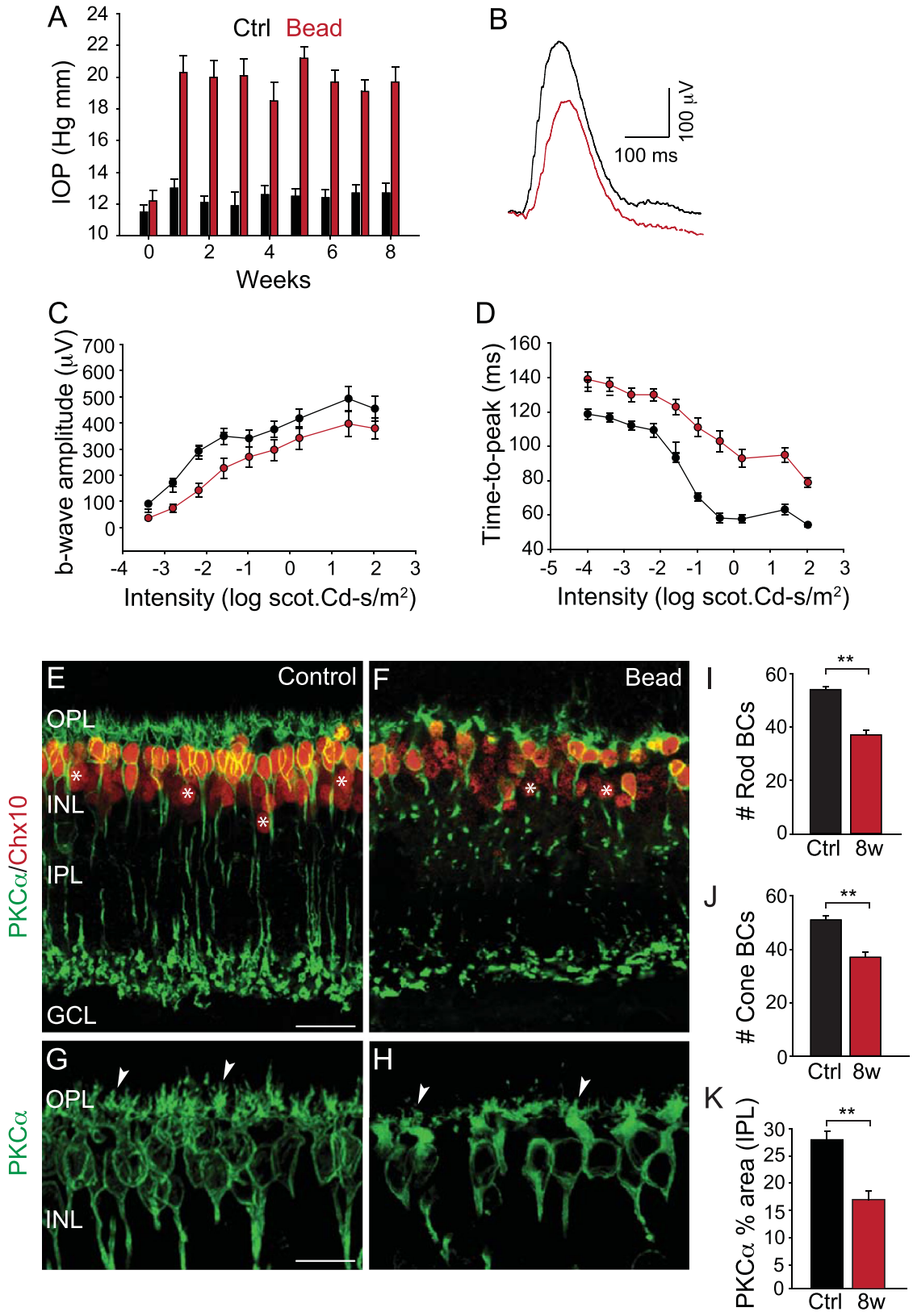


**Figure 1.** Effect of elevated IOP on bipolar cell structure and function in the C57BL/6 WT mouse. (**A**) Intraocular injection of microbeads (Bead) at weeks 0 and 4 results in a sustained elevation of IOP throughout the 8-week period as compared with sham-injected control (Ctrl) eyes. $^{***}P < 0.001$ for all time points; $n = 10$ eyes/group. (**B**) Example recordings show the b-waves of scotopic ERGs from WT mice under control conditions (*black*) and at 8 weeks after the initial microbead injection (*red*). There was a significant decrease of the peak amplitude (**C**) and an elevation of the time-to-peak latency (**D**) of the b-wave in glaucomatous eyes as compared with controls. Data are presented as mean ± SEM. $P < 0.05$ for all intensities; $n = 5$ eyes/group. (**E–H**) Confocal images of vertical sections from control and glaucomatous

Investigative Ophthalmology & Visual Science

retinas at 8 weeks after the initial microbead injection immunostained with anti-PKCα for rod BCs and anti-Chx10 for cone BCs (*asterisks*). *Arrowheads* in **G** and **H** show rod BC dendrites. Projection of eight images, $z = 0.7$ µm. (**I, J**) Histograms quantify the reduction of rod and cone BCs (per 300-µm lateral distance) in microbead-injected eyes, 8 weeks after initial injection, compared with controls. Data are presented as mean ± SEM. $^{**}P < 0.01$; $n = 5$ eyes/group. (**K**) Histogram showing the density of rod BC axon terminals in IPL of glaucomatous retinas as compared with control eyes. Data are presented as mean ± SEM. $^{**}P < 0.01$; $n = 5$ eyes/group. *Scale bar*: 10 µm in all panels. OPL, outer plexiform layer; INL, inner nuclear layer; IP, inner plexiform layer; GCL, ganglion cell layer.

scotopic ERGs weekly for 8 weeks following the initial microbead injection. Comparisons were made to control recordings from contralateral eyes with sham injections, as well as eyes from completely untreated animals. We found no significant differences in amplitude and shape of ERG waveforms obtained from the two control cohorts ($P > 0.1$ for both parameters). We analyzed the a-wave and b-wave profiles of the ERGs to evaluate changes in photoreceptor and BC function, respectively.[33,34] At 8 weeks after microbead injection, we found no significant change in the amplitude of the a-wave ($P > 0.1$; data not shown). Consistent with this finding, photoreceptor nuclei stained with 4′,6-diamidino-2-phenylindole showed no apparent loss in glaucomatous eyes ($P > 0.1$; data not shown). In contrast, elevation of IOP in WT mice resulted in a significant reduction in amplitude (Figs. 1B, 1C) and implicit time to peak (Fig. 1D) of the b-wave ($P < 0.05$; $n = 5$ eyes/group), indicative of changes in ON BC activity.[35]

Next, we assessed structural changes in BC structure in glaucomatous eyes. Vertical retinal sections of control and microbead-injected eyes from WT mice were immunostained with anti-PKCα, a selective marker for rod BCs (RBCs).[36–38] We then double-labeled retinas with anti-Chx10 to visualize BC nuclei.[36,39] Cone BCs (CBCs) were differentiable as Chx10-positive/PKCα-negative profiles (Figs. 1E, 1F). Under the control condition, PKCα-positive RBC somata formed two or three cell layers at the outer inner nuclear layer (INL) border with long, bushy dendrites (Figs. 1E, 1G). The RBC axons ended deep in layer 5 of the IPL as dense terminals with lateral varicosities (Fig. 1E). In glaucomatous retinas, we found a significant reduction in the number of RBC somata that, in contrast to controls, were mainly confined to a single layer adjacent to the outer plexiform layer (OPL) (Figs. 1F, 1I). We observed a 32% loss ($P < 0.001$; $n = 8$ eyes/group) at 8 weeks after microbead injection. The overall density and size of RBC axon terminals were reduced in glaucomatous eyes and showed a substantial reduction in the number of lateral varicosities ($P < 0.001$; $n = 8$ eyes/group) (Fig. 1K). There was also a marked loss of CBCs in glaucomatous eyes. We observed a 12% loss of cone BCs ($P < 0.05$; $n = 3$–5 eyes/group) by 5 weeks, which increased to a 22% loss ($P < 0.001$; $n = 8$ eyes/group) by 8 weeks.

## Timing of Bipolar Cell Structural Changes in Glaucoma

We have reported that the first significant loss of RGCs and amacrine cells (ACs) occurs at 4 weeks after initial microbead injection.[32] In the next series of experiments, we examined BC structure at weekly intervals after microbead injection to compare the time course with changes in the inner retina. The first significant loss of RBCs, a 13% reduction from control values ($P < 0.05$; $n = 3$–5 eyes/group), was at 4 weeks (Figs. 2A, 2C, 2E, 2G, 2M), whereas a significant loss of CBCs, a 12% reduction ($P < 0.01$; $n = 3$–5 eyes/group), first occurred at 5 weeks after microbead injection (Fig. 2N).

Prior to complete cell loss, neurons show structural changes to dendrites and axon terminals.[40,41] We have reported that αRGCs in glaucomatous mouse eyes that survive at 8 weeks show a significant loss of dendrites.[28] We extended this finding by calculating the dendritic lengths of anti-SMI32–labeled αRGCs at weekly intervals after microbead injection. We found the first significant change in dendritic length at 3 weeks, a 40% reduction from control values ($P < 0.01$; $n = 3$–5 eyes/group) (Figs. 2I–2L, 2P). In contrast, the first significant loss of RBC axon terminals was a 20% reduction ($P < 0.01$; $n = 3$–5 eyes/group) at 4 weeks (Figs. 2B, 2D, 2F, 2H, 2O). Clearly, early structural changes of RGC dendrites preceded those of BC axon terminals.

## Neuroprotection of the Outer Retina in Glaucoma

To test whether the BC changes were a consequence of prior degenerative changes in the inner retina, we leveraged the neuroprotective actions of GJ blockade or ablation reported in a number of retinopathies, including glaucoma.[28,31,32,42–44] We showed previously that selective genetic deletion of connexin 36 (Cx36) protein largely prevented loss of RGCs and ACs, preserved optic nerve axons, and reduced reactive gliosis in a mouse model of glaucoma.[28] Importantly, this neuroprotective action was not associated with a lowering of IOP.

We examined $Cx36^{+/+}$ and $Cx36^{-/-}$ mouse retinas under control and microbead injection conditions. The microbead injections elevated IOP for 8 weeks in eyes of $Cx36^{+/+}$ and $Cx36^{-/-}$ mice, similar to that described above for C57Bl/6 WT mice (Fig. 3A). Scotopic ERGs recorded from microbead-injected $Cx36^{+/+}$ eyes showed a significant reduction of the b-wave amplitude ($P < 0.001$; $n = 5$ eyes/group) (Fig. 3B). In contrast, we found no difference in b-wave amplitude or time to peak of $Cx36^{-/-}$ eyes under control conditions or 8 weeks after microbead injection ($P > 0.5$; $n = 5$ eyes/group for both parameters) (Figs. 3B–3D). We also found no change in the number of RBCs in $Cx36^{-/-}$ mouse eyes ($P > 0.5$; $n = 5$ eyes/group) (Figs. 3F, 3I), nor in the structure of their dendrites or axon terminals ($P > 0.5$; $n = 5$ eyes/group) (Figs. 3H, 3J). Likewise, there was no change in the number of CBCs in microbead-injected $Cx36^{-/-}$ eyes ($P > 0.1$; $n = 5$ eyes/group) (Figs. 3F, 3K). Qualitatively similar protection was observed in microbead-injected eyes of $Cx36^{+/+}$ control mice treated with the GJ blocker MFA (data not shown). Thus, ablation or blockade of GJs, shown previously to protect inner retinal neurons,[28] also prevented the deleterious effects of glaucoma on BCs.

## Synaptic Changes Associated With Rod Bipolar Cells in Glaucomatous Retinas

We next examined changes in synaptic structures associated with RBC dendrites and axon terminals in microbead-injected eyes. Retinas of WT mice were double immunolabeled for PKCα and anti-CtBP2, an established

Investigative Ophthalmology & Visual Science

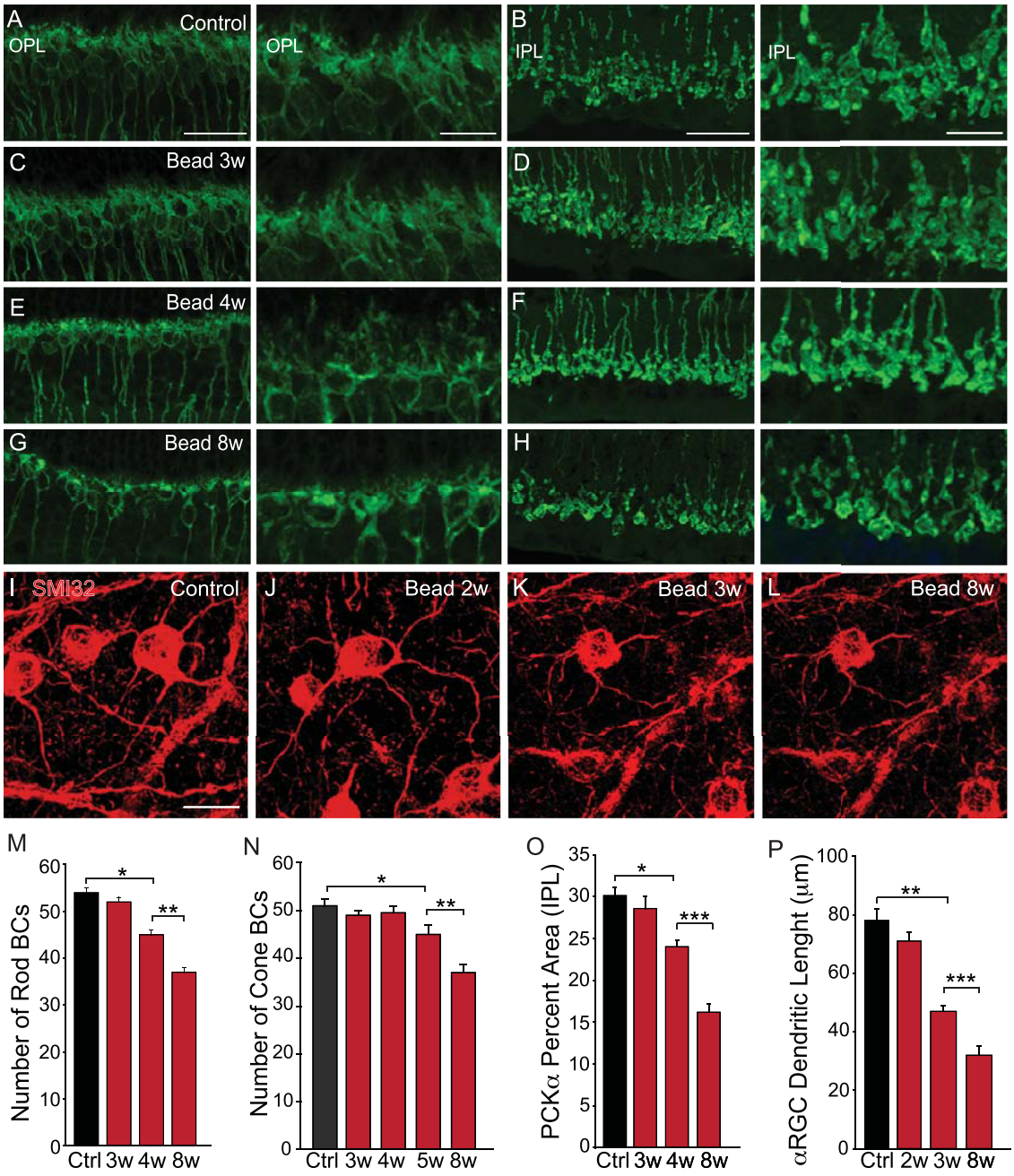


**Figure 2.** Time course of changes in bipolar cell morphology following IOP elevation by microbead injection. (**A**) Micrographs of vertical retinal sections at different magnifications from control eyes of rod BC somata and dendrites labeled with anti-PKC$\alpha$. *Scale bars*: 50 µm (*left*) and 15 µm (*right*). (**B**) Axon terminals of rod BCs in control eyes. *Scale bars*: 50 µm (*left*) and 15 µm (*right*). (**C**) Rod BC somata and dendrites at 3 weeks after initial microbead injection. (**D**) Rod BC axon terminals at 3 weeks after initial microbead injection. (**E**) Rod BC somata and dendrites 4 weeks after initial microbead injection. (**F**) Rod BC axon terminals at 4 weeks after initial microbead injection. (**G**) Rod BC somata and dendrites at 8 weeks after initial microbead injection. (**H**) Rod BC axon terminals at 8 weeks after initial microbead injection. (**I–L**) Images of retinal whole mounts immunolabeled for SMI32 to visualize $\alpha$RGC somata and dendrites under control conditions and at weekly timepoints after initial microbead injection. *Scale bar*: 20 µm. (**M**) Histogram showing the number of rod BC somata at different timepoints after initial microbead injection. (**N**) Number of cone BC somata at different timepoints after initial microbead injection. (**O**) Density of rod BC axon terminals in IPL of retinas at different time points after initial microbead injection. (**P**) Histogram quantifying dendritic lengths of $\alpha$RGCs in control retinas and at different time points after initial microbead injection. $^{*}P < 0.05$, $^{**}P < 0.01$, $^{***}P < 0.001$; $n = 5$ eyes for control data and $n = 3$ eyes for each weekly timepoint. Panels **A** to **H** are a projection of five images, $z = 1$ µm.

marker for photoreceptor synaptic ribbons.[45] For the first 3 weeks following microbead injection, the dendritic architecture of RBCs appeared similar to that in controls (Figs. 4A–4C). This included processes projecting to CtBP2-positive, horseshoe-shaped presynaptic ribbons (Fig. 4B, inset). However, structural changes in the OPL were first observed at 4 weeks and progressed over the next 4 weeks (Figs. 4D–4F). These changes included a retraction of dendrites and a 27% ($P < 0.01$, $n = 3$ eye/group) reduction in CtBP2-positive synaptic ribbons (Fig. 4J), with the spared ribbons

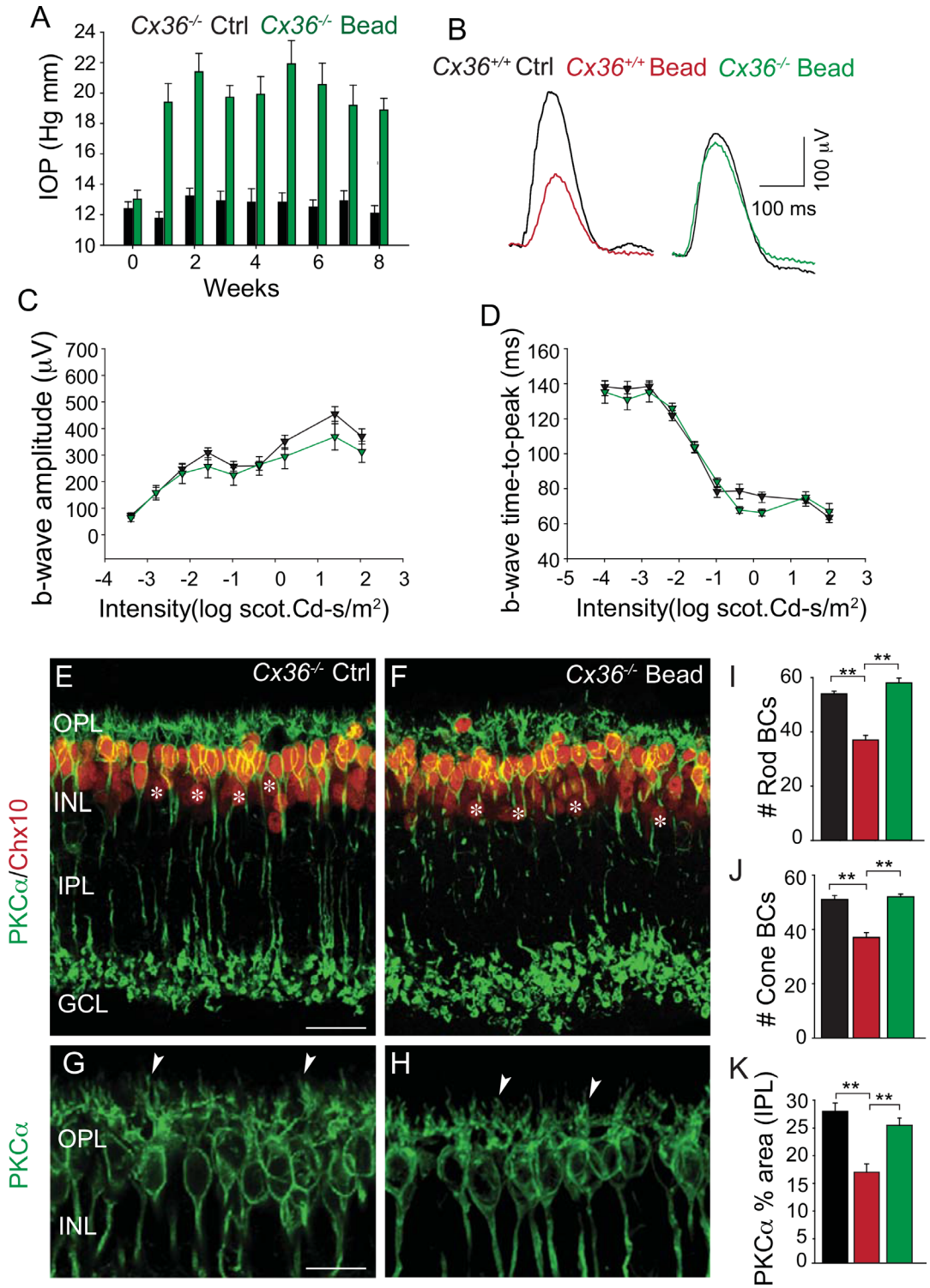


**Figure 3.** Effect of elevated IOP on BC structure and function in the *Cx36*$^{-/-}$ mouse. (**A**) Intraocular injection of microbeads at weeks 0 and 4 resulted in a sustained elevation of IOP throughout the 8-week period as compared with sham-injected control eyes. $^{***}P < 0.001$ for all time points; $n = 5$ eyes/group. (**B**) Example recordings showing that at 8 weeks after initial microbead injection the b-wave of the scotopic ERG was reduced in *Cx36*$^{+/+}$ mouse eyes but not in *Cx36*$^{-/-}$ mice (**C, D**) Scatterplots show that there was no change in the amplitude or time-to-peak latency of the ERG b-wave in glaucomatous eyes as compared with control eyes from *Cx36*$^{-/-}$ mice. $P > 0.5$; $n =$ 5 eye/group. (**E–H**) Confocal images of vertical sections from control and glaucomatous retinas at 8 weeks after initial microbead injection of *Cx36*$^{-/-}$ mice immunolabeled with anti-PKC*α* for rod BCs and anti-Chx10 for cone BCs (*asterisks*). *Arrowheads* show the preservation of rod BC dendrites in the OPL of microbead-injected *Cx36*$^{-/-}$ retinas. Projection of eight images; $z = 0.7$ µm. (**I, J**) Histograms comparing the reduction of rod and cone BCs (per 300-µm lateral distance) in microbead-injected *Cx36*$^{+/+}$ (*red*) and *Cx36*$^{-/-}$ mice (*green*) compared with control (*black*) levels. Data are presented as mean ± SEM. $^{**}P < 0.01$; $n = 5$ eyes/group. (**K**) Histogram quantifies the density of rod BC axon terminals in the IPL of glaucomatous *Cx36*$^{+/+}$ and *Cx36*$^{-/-}$ mice as compared with control eyes. Data are presented as mean ± SEM. $^{**}P < 0.01$; $n = 5$ eyes/group. *Scale bar*: 10 µm in all panels. Conventions are the same as in Figure 1.

Investigative Ophthalmology & Visual Science

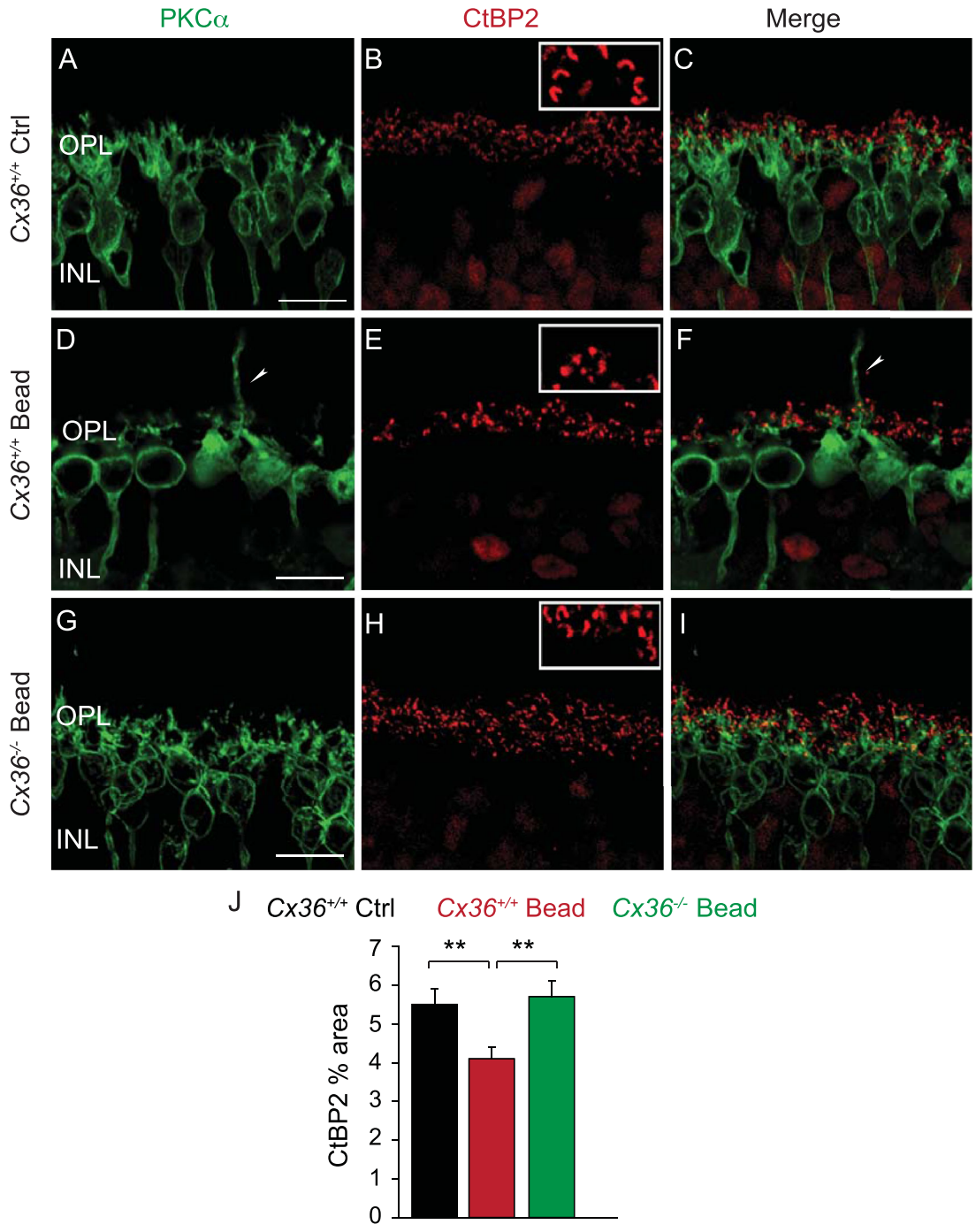


**Figure 4.** Ablation of *Cx36*-expressing GJs prevented changes in synaptic ribbon number and structure in the OPL of microbead-injected retinas. (**A–C**) Immunolabeling for PKCα to visualize dendrites of rod BCs and CtBP2 to visualize ribbon synapses in vertical retinal sections from control $Cx36^{+/+}$ mouse retinas. Inset in **B** shows the horseshoe shape of the ribbons. (**D–F**) Immunolabeling for PKCα to visualize dendrites of rod BCs and CtBP2 to visualize ribbon synapses in vertical retinal sections from control $Cx36^{+/+}$ mouse retinas 8 weeks after initial microbead injection. Inset in **E** shows the structural transformation of synaptic ribbons to a punctate shape, and *arrowheads* in **D** and **E** show the sprouting of BC dendrites in the ONL. (**G–I**) Immunolabeling for PKCα to visualize dendrites of rod BCs and CtBP2 to visualize ribbon synapses in vertical retinal sections from $Cx36^{-/-}$ mouse retinas 8 weeks after initial microbead injection. The structure of BC dendrites and synaptic ribbons is similar to that seen in control eyes. (**J**) Histogram showing that the reduced density of photoreceptor synaptic ribbons in glaucomatous eyes in control $Cx36^{+/+}$ mice was prevented in $Cx36^{-/-}$ mice. Data are presented as mean ± SEM. $^{**}P < 0.01$; $n = 3$ eyes/group. *Scale bar*: 10 µm in all panels. Conventions are the same as in Figure 1. Panels **A–I** are a projection of five images, $z = 0.7$ µm.

remodeled to a punctate shape (Fig. 4E, inset), which were no longer clearly associated with dendritic tips of RBCs. Despite these changes to the photoreceptor synaptic complex, there was no measurable loss of photoreceptors over the 8-week experimental period. We occasionally observed RBC dendrites sprouting (Figs. 4D, 4F), a process

Investigative Ophthalmology & Visual Science

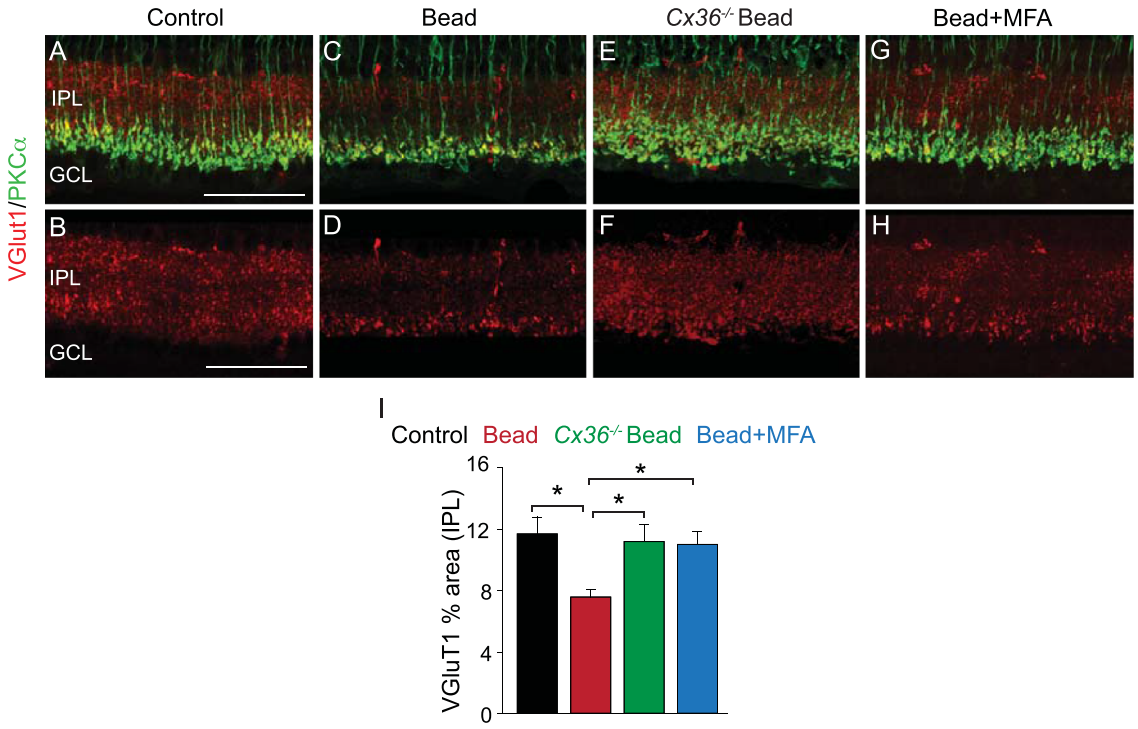


**Figure 5.** Reduction of VGluT1 immunoreactivity in the IPL of glaucomatous WT mouse retina was prevented by blockade of GJs with MFA or ablation of Cx36. (**A**, **B**) Retinal vertical sections from control WT mice immunolabeled for PKC$\alpha$ to visualize rod BC axon terminals in the IPL and VGluT1 to visualize glutamate transporters in BC presynaptic terminals. (**C**, **D**) At 8 weeks after initial microbead injection, the density of VGluT1 label was markedly reduced in WT retinas. (**E**, **F**) In contrast, immunolabels at 8 weeks after initial microbead injection into *Cx36*$^{-/-}$ mouse eyes were similar to those seen in control retinas. (**G**, **H**) At 8 weeks after initial microbead injection, WT eyes injected with the GJ blocker MFA also showed immunolabeling comparable to that in control eyes. (**I**) Histogram quantifying density of VGluT1 immunolabeling under the different mouse strains and protocols. Data are presented as mean ± SEM. $^{*}P < 0.05$; $n = 4$ eyes/group. *Scale bar*: 10 µm in all panels. All panels are a projection of seven images; $z = 0.7$ µm. Conventions are the same as in Figure 1.

of remodeling,[46,47] presumably to make ectopic contact with photoreceptor terminals. In contrast, we observed no significant changes in RBC dendritic structure, nor in the number and shape of the CtBP2-positive synaptic ribbons, in the OPL of microbead-injected *Cx36*$^{-/-}$ mice (Figs. 4G–4J).

We next investigated changes in the distribution of vesicular glutamate transporter 1 (VGluT1) in glaucomatous eyes, which is responsible for the uploading of glutamate into synaptic vesicles.[48] Consistent with earlier studies,[49,50] immunostaining of control retinas (Fig. 5A) showed discrete punctate labeling for VGluT1 throughout the IPL (Fig. 5B). Double-labeling experiments identified large PKC$\alpha$-positive RBC axon terminals in distal layer 5 of the IPL with VGluT1 expression (Fig. 5A). In glaucomatous retinas, the density of VGluT1-positive structures was reduced in the IPL by 34% ($P < 0.05$; $n = 4$ eyes/group) (Figs. 5C, 5D, 5I). This reduction was evident for VGluT1-positive patches that were colocalized with the PKC$\alpha$-positive terminals deep in layer 5 of the IPL (Fig. 5E). The reduced VGluT1 expression throughout both sublamina in the IPL strongly suggests synaptic changes to CBC axon terminals, as well.

In contrast, we observed no significant change in the pattern of VGluT1 immunolabeling in microbead-injected *Cx36*$^{-/-}$ mice (Figs. 5E, 5F, 5I). Similarly, pharmacological block of GJs by application of MFA prevented changes in VGluT1 expression in microbead-injected WT mouse retinas over the 8-week experimental period (Figs. 5G–5I).

## Altered Morphology of Horizontal Cells in Glaucomatous Retinas

A single type of axon-bearing HCs in mouse makes synaptic contacts with cone and rod photoreceptors via dendritic and axonal endings, respectively.[51,52] The HCs form an electrically coupled network important to contrast sensitivity,[53] a feature often impaired in glaucoma patients.[54,55] We therefore looked for morphological changes in HC structure in glaucomatous retinas by labeling vertical sections with anti-calbindin (CB)[37] (Fig. 6A). We found no significant difference between the number of HC somata in control retinas and those in microbead-injected eyes ($P > 0.5$; $n = 3$ eyes/group), but we did see structural changes in dendritic and axonal processes. In addition to the thick proximal dendritic processes, distal punctate terminal endings could be visualized at the level of photoreceptor terminals (arrowheads). However, we found that to see the terminal puncta it was necessary to increase the gain of the photomultiplier of the confocal microscope, which resulted in a saturated image. Although these synaptic terminals have been described previously as dendritic tips,[16] it is possible that some puncta may be axon terminals. Nevertheless, at 8 weeks after microbead injection, we found that CB-positive terminal puncta showed a clear change in structure (Fig. 6B). Although background CB label could be visualized, there was a clear loss of the punctate structure seen in control retinas. In contrast, retinas from microbead-injected eyes of

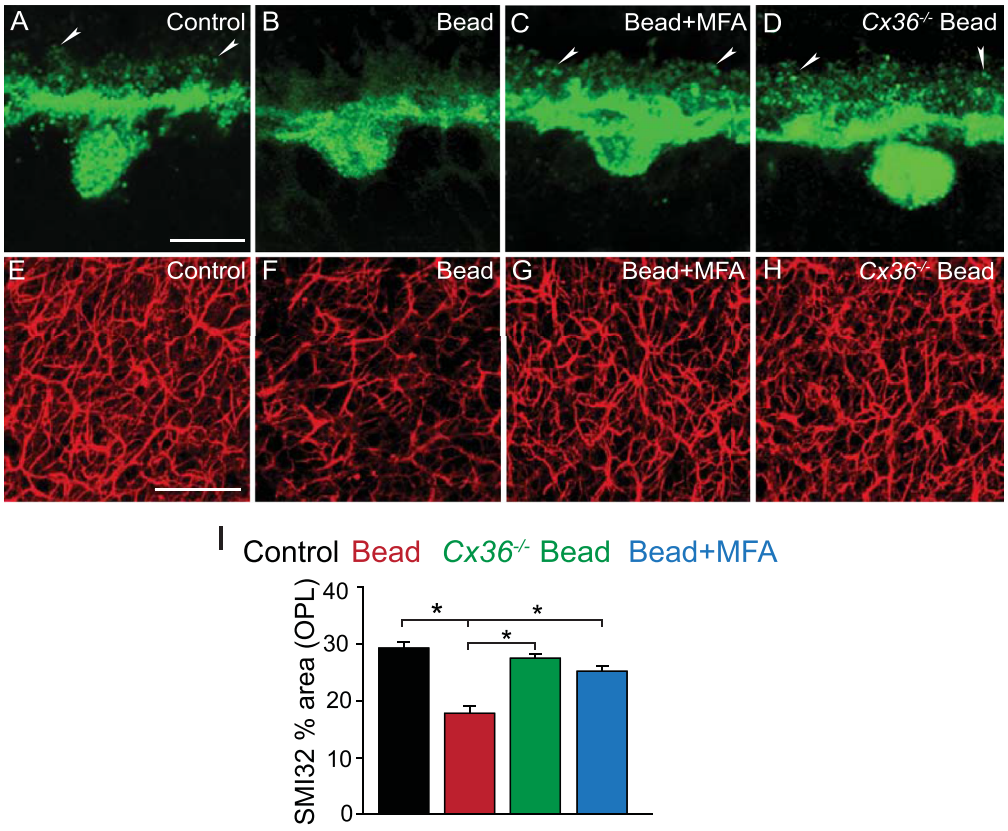


**Figure 6.** Remodeling of horizontal cell dendrites and axon terminals in glaucomatous eyes was prevented by GJ blockade with MFA or ablation of Cx36. (**A**, **B**) Retinas from control WT eyes immunolabeled with anti-calbindin (CB) to visualize HC somata and dendrites in vertical sections and anti-SMI32 to visualize HC axon terminals in whole mounts. *Arrowheads* point to beaded synaptic endings presumably from dendrites. (**C**, **D**) At 8 weeks after initial microbead injection, there were structural changes in WT mouse retinas in terms of the visible structure of synaptic endings and the density of axon terminals. (**E**, **F**) At 8 weeks after initial microbead injection, the HC dendritic and axon terminal structure in *Cx36*$^{-/-}$ mouse retinas was comparable to that seen in control eyes. (**G**, **H**) Similarly, at 8 weeks after initial microbead injection, WT mouse eyes treated with MFA showed HC structure comparable to that in control eyes. (**I**) Histogram quantifies changes in the density of HC axon terminals in different mouse strains and protocols. Data in panels **I** and **J** are presented as mean ± SEM. $^{**}P < 0.01$, $^{*}P < 0.05$; $n = 3$ eyes/group. *Scale bar*: 10 µm in the *top* panels and 20 µm in the *bottom* panels. Panels **A** to **D** are the projection of five images; $z = 0.7$ µm. Conventions are the same as in Figure 1.

*Cx36*$^{-/-}$ mice or WT mice treated with MFA maintained the punctate structure of terminal endings seen in control retinas (Figs. 6C, 6D).

The axon terminals of HCs in mouse retina express a non-phosphorylated neurofilament, which can be visualized by anti-SMI32 labeling.[52,56] The OPL of control retinas contained an extensive meshwork of laterally arborizing processes of HC axon terminals[52] (Fig. 6B). In contrast, the coverage of SMI32-positive axon terminals was reduced by 39% ($P < 0.05$; $n = 3$ eyes/group) in glaucomatous retinas with spared processes that were shorter and less ramified than controls (Figs. 6D, 6J). In contrast, retinas from microbead-injected *Cx36*$^{-/-}$ (Fig. 6F) or MFA-treated WT (Fig. 6H) mice showed no significant changes ($P > 0.5$; $n = 3$ eyes/group) in density or appearance of SMI32-positive axon terminals (Fig. 6J).

## Discussion

Despite findings of abnormalities in the outer retina of human patients and animal models with glaucoma,[9,14] it has remained unclear whether these changes result directly from glaucomatous insult or are secondary consequences of inner retinal pathology.[25] Our findings support and extend the evidence for outer retinal damage in experimental glaucoma but also provide strong evidence that outer retinal changes occur subsequent to and result as a consequence of inner retinal damage.

Consistent with earlier glaucoma studies,[10,14,57–61] we found that sustained elevation of IOP negatively affected the ERG b-wave in WT mice, suggesting a reduction of ON BC activity.[35] We found a corresponding loss of both RBCs and CBCs in glaucomatous eyes. A loss of RBC immunoreactivity for PKC$\alpha$ has been reported earlier in a vein cauterization model of glaucoma in rats, but it was not clear whether these cells died or had stopped expressing the molecular marker.[13] The decreased number of PKC$\alpha$-positive RBCs, as well as Chx10-positive CBCs, in our study is most likely attributable to cell death rather than a change in protein expression, as surviving BCs showed intensity of immunolabeling comparable to that in control retinas. Structural changes to dendrites and axon terminals have been reported in a number of ocular pathologies, including glaucoma.[14,46,62–67] Consistent with these studies, we found that dendrites of surviving RBCs were less profuse than in controls, with some cells almost devoid of processes. In the IPL, RBC axon terminals showed decreased branching with smaller varicosities, similar to

changes described in the DBA/2J mouse model of congenital glaucoma.[66]

We observed a significant alteration in CtBP2 immunostaining in the OPL in glaucomatous retinas, indicating damage to the photoreceptor synaptic complex. Such changes corresponded to dendritic changes of second-order BCs and HCs, which included retraction of tip processes and occasional abnormal growth. The morphological alterations of structures in the OPL are consistent with the functional impairment indicated by changes in the ERG b-wave. In the IPL, surviving RBC axon terminal endings in glaucomatous retinas retained PKC$\alpha$ expression but lost the VGluT1 immunoreactivity found in control retinas. This suggests that synaptic release of glutamate from BCs to postsynaptic targets is diminished, as well.

The first significant loss of RBCs was first observed 4 weeks after microbead injection, which coincides with the earliest reported loss of RGCs and ACs.[28,32] In contrast, significant loss of CBCs was first seen at 5 weeks after microbead injection. Changes in dendritic architecture preceding neuronal loss have been described in animal models of glaucoma.[40,41] We found significant loss of dendritic processes in RGCs as early as 3 weeks after the initial microbead injection. However, damage to RBC axon terminals was first observed at 4 weeks, a significant difference in timing relative to our 8-week model.

Overall, these findings support the idea that structural changes to outer retinal neurons occur subsequent to those in the inner retina but do not address whether they result as a consequence. To examine this question, we determined whether neuroprotection of inner retinal neurons could also prevent damage in the outer retina. Indeed, we found that genetic ablation of Cx36 or blockade of GJs with MFA prevented structural damage to BCs and HCs, preserved the ERG b-wave at control levels, and sustained synaptic structures in the OPL and IPL of glaucomatous retinas. Combined with our previous finding that ablation of Cx36-expressing GJs protects RGCs and ACs,[28] these results support the idea that outer retina damage is a secondary consequence of inner retinal pathology in glaucoma. Yet, the question may still be raised whether GJ blockade or, in particular, Cx36 ablation could directly protect the outer retina independent of actions in the inner retina. A number of points argue against this possibility. First, HC GJs in the mouse retina express Cx57 but not Cx36.[68] Second, although photoreceptors do express Cx36,[69] our finding of no significant loss in glaucoma indicates that bystander cell death did not occur at the ONL level. Third, RBCs do not express GJs. Fourth, although some OFF CBCs may express Cx36,[70] ON CBCs mainly express Cx45[71,72] and are coupled to glycinergic AII ACs,[73,74] which are relatively unaffected in the glaucoma mouse model.[32] These findings thus strongly suggest that bystander-mediated neuronal loss occurred exclusively in the inner retina. Our conclusion that outer retinal damage follows that in the inner retina is supported by the findings for glaucoma patients and DBA/2J mice that outer retina damage was found prominently in regions overlying patches of inner retina with prominent RGC loss.[8,16,25]

The mechanism by which damage to the inner retina in glaucoma can lead to changes in outer retina is unclear. However, as BCs are presynaptic to vulnerable RGCs and ACs, a likely mechanism is trans-neuronal or trans-synaptic degeneration.[27,75,76] In this scheme, the degeneration of BCs does not result from the primary insult but rather from the loss of their postsynaptic target cells, consistent with attenuated VGluT1 expression in BC axon terminals. This mechanism has been linked to cell death in numerous CNS neurological diseases, including recently in glaucoma.[27,77–79] Although CBCs synapse directly with degenerating RGCs, RBCs do not; however, RBCs make synaptic contacts with ACs, which have been shown to degenerate in glaucomatous eyes with a time course similar to that for the loss of RGCs.[28] In turn, the structural changes in BC dendrites could then lead to the observed alterations in photoreceptor terminal synaptic complexes that, in turn, initiate the postsynaptic degeneration of HC dendritic and axonal processes.

Another potential mechanism for the spread of retinal damage is reactive gliosis, which is often manifested as an increase in glial fibrillary acidic protein expression in astrocytes lying adjacent to the nerve fiber layer and in Müller cell processes that extend vertically through retinal layers.[28,80,81] Reactive gliosis can alter environmental homeostasis and release toxins that can lead to progressive neuronal degeneration.[82,83] Interestingly, ablation of Cx36 or blockade of GJs, which we show here can prevent outer retinal changes in glaucoma, has been reported to prevent gliosis.[28]

Although IOP-lowering drugs remain the mainstay treatment for glaucoma, recent studies have turned to neuroprotective strategies to prevent cell death and subsequent vision loss.[84] Importantly, therapies providing protection to the inner retina but leaving outer retinal damage unaffected would be pointless, as dysfunctional BC signaling to RGCs would still lead to vision defects. It is therefore fortuitous that our findings show that protection of the inner retina by GJ blockade can also prevent damage to outer retinal neurons, including their synaptic connections. Our findings thus reveal inner retinal neurons as potential targets for effective neuroprotective therapies to sustain vision in glaucoma patients.

## *Acknowledgments*

Supported by grants from the National Institutes of Health (EY026024 and EY007360 to S.A.B.).

Disclosure: **S. Kumar**, None; **H. Ramakrishnan**, None; **S. Viswanathan**, None; **A. Akopian**, None; **S.A. Bloomfield**, Research Foundation (P), Connexin Therapeutics (I)

## *References*

1. Quigley HA. Neuronal death in glaucoma. *Prog Retin Eye Res*. 1999;18(1):39–57.
2. Schwartz M. Neurodegeneration and neuroprotection in glaucoma: development of a therapeutic neuroprotective vaccine: the Friedenwald lecture. *Invest Ophthalmol Vis Sci*. 2003;44(4):1407–1411.
3. Kendell KR, Quigley HA, Kerrigan LA, Pease ME, Quigley EN. Primary open-angle glaucoma is not associated with photoreceptor loss. *Invest Ophthalmol Vis Sci*. 1995;36(1):200–205.
4. Frishman LJ, Shen FF, Du L, et al. The scotopic electroretinogram of macaque after retinal ganglion cell loss from experimental glaucoma. *Invest Ophthalmol Vis Sci*. 1996;37(1):125–141.
5. Levkovitch-Verbin H, Quigley HA, Martin KR, Valenta D, Baumrind LA, Pease ME. Translimbal laser photocoagulation to the trabecular meshwork as a model of glaucoma in rats. *Invest Ophthalmol Vis Sci*. 2002;43(2):402–410.
6. Cifuentes-Canorea P, Ruiz-Medrano J, Gutierrez-Bonet R, et al. Analysis of inner and outer retinal layers using

spectral domain optical coherence tomography automated segmentation software in ocular hypertensive and glaucoma patients. *PLoS One*. 2018;13(4):e0196112.

7. Nork TM, Ver Hoeve JN, Poulsen GL, et al. Swelling and loss of photoreceptors in chronic human and experimental glaucomas. *Arch Ophthalmol*. 2000;118(2):235–245.
8. Lei Y, Garrahan N, Hermann B, et al. Quantification of retinal transneuronal degeneration in human glaucoma: a novel multiphoton-DAPI approach. *Invest Ophthalmol Vis Sci*. 2008;49(5):1940–1945.
9. Choi SS, Zawadzki RJ, Lim MC, et al. Evidence of outer retinal changes in glaucoma patients as revealed by ultrahigh-resolution in vivo retinal imaging. *Br J Ophthalmol*. 2011;95(1):131–141.
10. Georgiou AL, Guo L, Francesca Cordeiro M, Salt TE. Electroretinogram and visual-evoked potential assessment of retinal and central visual function in a rat ocular hypertension model of glaucoma. *Curr Eye Res*. 2014;39(5):472–486.
11. Ortín-Martínez A, Salinas-Navarro M, Nadal-Nicolás FM, et al. Laser-induced ocular hypertension in adult rats does not affect non-RGC neurons in the ganglion cell layer but results in protracted severe loss of cone-photoreceptors. *Exp Eye Res*. 2015;132:17–33.
12. Velten IM, Horn FK, Korth M, Velten K. The b-wave of the dark adapted flash electroretinogram in patients with advanced asymmetrical glaucoma and normal subjects. *Br J Ophthalmol*. 2001;85(4):403–409.
13. Hernandez M, Rodriguez FD, Sharma SC, Vecino E. Immunohistochemical changes in rat retinas at various time periods of elevated intraocular pressure. *Mol Vis*. 2009;15:2696–2709.
14. Cuenca N, Pinilla I, Fernández-Sánchez L, et al. Changes in the inner and outer retinal layers after acute increase of the intraocular pressure in adult albino Swiss mice. *Exp Eye Res*. 2010;91(2):273–285.
15. Cuenca N, Fernández-Sánchez L, Campello L, et al. Cellular responses following retinal injuries and therapeutic approaches for neurodegenerative diseases. *Prog Retin Eye Res*. 2014;43:17–75.
16. Fernández-Sánchez L, de Sevilla Müller LP, Brecha NC, Cuenca N. Loss of outer retinal neurons and circuitry alterations in the DBA/2J mouse. *Invest Ophthalmol Vis Sci*. 2014;55(9):6059–6072.
17. Pang JJ, Frankfort BJ, Gross RL, Wu SM. Elevated intraocular pressure decreases response sensitivity of inner retinal neurons in experimental glaucoma mice. *Proc Natl Acad Sci USA*. 2015;112(8):2593–2598.
18. Janssen P, Naskar R, Moore S, Thanos S, Thiel HJ. Evidence for glaucoma-induced horizontal cell alterations in the human retina. *Ger J Ophthalmol*. 1996;5(6):378–385.
19. Euler T, Haverkamp S, Schubert T, Baden T. Retinal bipolar cells: elementary building blocks of vision. *Nat Rev Neurosci*. 2014;15(8):507–519.
20. Chaya T, Matsumoto A, Sugita Y, et al. Versatile functional roles of horizontal cells in the retinal circuit. *Sci Rep*. 2017;7(1):1–15.
21. Ströh S, Puller C, Swirski S, et al. Eliminating glutamatergic input onto horizontal cells changes the dynamic range and receptive field organization of mouse retinal ganglion cells. *J Neurosci*. 2018;38(8):2015–2028.
22. Kalloniatis M, Harwerth RS, 3rd Smith EL, DeSantis L. Colour vision anomalies following experimental glaucoma in monkeys. *Ophthalmic Physiol Opt*. 1993;13(1):56–67.
23. Sabharwal J, Seilheimer RL, Tao X, Cowan CS, Frankfort BJ, Wu SM. Elevated IOP alters the space-time profiles in the center and surround of both ON and OFF RGCs in mouse. *Proc Natl Acad Sci USA*. 2017;114(33):8859–8864.
24. Shakarchi AF, Mihailovic A, West SK, Friedman DS, Ramulu PY. Vision parameters most important to functionality in glaucoma. *Invest Ophthalmol Vis Sci*. 2019;60(14):4556–4563.
25. Werner JS, Keltner JL, Zawadzki RJ, Choi SS. Outer retinal abnormalities associated with inner retinal pathology in nonglaucomatous and glaucomatous optic neuropathies. *Eye (Lond)*. 2011;25(3):279–289.
26. Calkins DJ. Critical pathogenic events underlying progression of neurodegeneration in glaucoma. *Prog Retin Eye Res*. 2012;31(6):702–719.
27. Lawlor M, Danesh-Meyer H, Levin LA, Davagnanam I, De Vita E, Plant GT. Glaucoma and the brain: trans-synaptic degeneration, structural change, and implications for neuroprotection. *Surv Ophthalmol*. 2018;63(3):296–306.
28. Akopian A, Kumar S, Ramakrishnan H, Roy K, Viswanathan S, Bloomfield SA. Targeting neuronal gap junctions in mouse retina offers neuroprotection in glaucoma. *J Clin Invest*. 2017;127(7):2647–2661.
29. Deans MR, Volgyi B, Goodenough DA, Bloomfield SA, Paul DL. Connexin36 is essential for transmission of rod-mediated visual signals in the mammalian retina. *Neuron*. 2002;36(4):703–712.
30. Sappington RM, Carlson BJ, Crish SD, Calkins DJ. The microbead occlusion model: a paradigm for induced ocular hypertension in rats and mice. *Invest Ophthalmol Vis Sci*. 2010;51(1):207–216.
31. Akopian A, Atlasz T, Pan F, et al. Gap junction-mediated death of retinal neurons is connexin and insult specific: a potential target for neuroprotection. *J Neurosci*. 2014;34(32):10582–10591.
32. Akopian A, Kumar S, H, Viswanathan S, Bloomfield SA. Amacrine cells coupled to ganglion cells via gap junctions are highly vulnerable in glaucomatous mouse retinas. *J Comp Neurol*. 2019;527(1):159–173.
33. Penn RD, Hagins WA. Signal transmission along retinal rods and the origin of the electroretinographic a-wave. *Nature*. 1969;223(5202):201–205.
34. Robson JG, Frishman LJ. Response linearity and kinetics of the cat retina: the bipolar cell component of the dark-adapted electroretinogram. *Vis Neurosci*. 1995;12(5):837–850.
35. Stockton RA, Slaughter MM. B-wave of the electroretinogram. A reflection of ON bipolar cell activity. *J Gen Physiol*. 1989;93(1):101–122.
36. Greferath U, Grünert U, Wässle H. Rod bipolar cells in the mammalian retina show protein kinase C-like immunoreactivity. *J Comp Neurol*. 1990;301(3):433–442.
37. Haverkamp S, Wässle H. Immunocytochemical analysis of the mouse retina. *J Comp Neurol*. 2000;424(1):1–23.
38. Morrow EM, Chen CM, Cepko CL. Temporal order of bipolar cell genesis in the neural retina. *Neural Dev*. 2008;3(1):1–9.
39. Burmeister M, Novak J, Liang MY, et al. Ocular retardation mouse caused by Chx10 homeobox null allele: impaired retinal progenitor proliferation and bipolar cell differentiation. *Nat Genet*. 1996;12(4):376–384.
40. Morgan JE, Datta AV, Erichsen JT, Albon J, Boulton ME. Retinal ganglion cell remodelling in experimental glaucoma. *Adv Exp Med Biol*. 2006;572:397–402.
41. El-Danaf RN, Huberman ADJ. Characteristic patterns of dendritic remodeling in early-stage glaucoma: evidence from genetically identified retinal ganglion cell types. *J Neurosci*. 2015;35(6):2329–2343.
42. Spray DC, Hanstein R, Lopez-Quintero SV, Stout RF, Suadicani SO, Thi MM. Gap junctions and bystander effects: Good Samaritans and executioners. *Wiley Interdiscip Rev Membr Transp Signal*. 2013;2(1):1–15.

Investigative Ophthalmology & Visual Science

43. Danesh-Meyer HV, Zhang J, Acosta ML, Rupenthal ID, Green CR. Connexin43 in retinal injury and disease. *Prog Retin Eye Res*. 2016;51:41–68.
44. O'Brien J, Bloomfield SA. Plasticity of retinal gap junctions: roles in synaptic physiology and disease. *Annu Rev Vis Sci*. 2018;4:79–100.
45. Dieck S, Altrock WD, Kessels MM, et al. Molecular dissection of the photoreceptor ribbon synapse: physical interaction of Bassoon and RIBEYE is essential for the assembly of the ribbon complex. *J Cell Biol*. 2005;168(5):825–836.
46. Cuenca N, Pinilla I, Sauvé Y, Lu B, Wang S, Lund RD. Regressive and reactive changes in the connectivity patterns of rod and cone pathways of P23H transgenic rat retina. *Neuroscience*. 2004;127(2):301–317.
47. Liets LC, Eliasieh K, Van Der List DA, Chalupa LM. Dendrites of rod bipolar cells sprout in normal aging retina. *Proc Natl Acad Sci USA*. 2006;103(32):12156–12160.
48. Sherry DM, Wang MM, Bates J, Frishman LJ. Expression of vesicular glutamate transporter 1 in the mouse retina reveals temporal ordering in development of rod vs. cone and ON vs. OFF circuits. *J Comp Neurol*. 2003;465(4):480–498.
49. Johnson J, Tian N, Caywood MS, Reimer RJ, Edwards RH, Copenhagen DR. Vesicular neurotransmitter transporter expression in developing postnatal rodent retina: GABA and glycine precede glutamate. *J Neurosci*. 2003;23(2):518–529.
50. Haverkamp S, Ghosh KK, Hirano AA, Wässle H. Immunocytochemical description of five bipolar cell types of the mouse retina. *J Comp Neurol*. 2003;455(4):463–476.
51. Kolb H. The connections between horizontal cells and photoreceptors in the retina of the cat: electron microscopy of Golgi preparations. *J Comp Neurol*. 1974;155(1):1–14.
52. Peichl L, González-Soriano J. Morphological types of horizontal cell in rodent retinae: a comparison of rat, mouse, gerbil, and guinea pig. *Vis Neurosci*. 1994;11(3):501–517.
53. Lipin MY, Smith RG, Taylor WR. Maximizing contrast resolution in the outer retina of mammals. *Biol Cybern*. 2010;103(1):57–77.
54. Hawkins AS, Szlyk JP, Ardickas Z, Alexander KR, Wilensky JT. Comparison of contrast sensitivity, visual acuity, and Humphrey visual field testing in patients with glaucoma. *J Glaucoma*. 2003;12(2):134–138.
55. Hu CX, Zangalli C, Hsieh M, et al. What do patients with glaucoma see? Visual symptoms reported by patients with glaucoma. *Am J Med Sci*. 2014;348(5):403–409.
56. Strettoi E, Pignatelli V. Modifications of retinal neurons in a mouse model of retinitis pigmentosa. *Proc Natl Acad Sci USA*. 2000;97(20):11020–11025.
57. Holopigian K, Seiple W, Mayron C, Koty R, Lorenzo M. Electrophysiological and psychophysical flicker sensitivity in patients with primary open-angle glaucoma and ocular hypertension. *Invest Ophthalmol Vis Sci*. 1990;31(9):1863–1868.
58. Bayer AU, Danias J, Brodie S, et al. Electroretinographic abnormalities in a rat glaucoma model with chronic elevated intraocular pressure. *Exp Eye Res*. 2001;72(6):667–677.
59. Harazny J, Scholz M, Buder T, Lausen B, Kremers J. Electrophysiological deficits in the retina of the DBA/2J mouse. *Doc Ophthalmol*. 2009;119(3):181–197.
60. Salinas-Navarro M, Alarcón-Martínez L, Valiente-Soriano FJ, et al. Functional and morphological effects of laser-induced ocular hypertension in retinas of adult albino Swiss mice. *Mol Vis*. 2009;15:2578–2598.
61. Domenici L, Origlia N, Falsini B, et al. Rescue of retinal function by BDNF in a mouse model of glaucoma. *PLoS One*. 2014;9(12):e115579.
62. Strettoi E, Pignatelli V, Rossi C, Porciatti V, Falsini B. Remodeling of second-order neurons in the retina of rd/rd mutant mice. *Vision Res*. 2003;43(8):867–877.
63. Barhoum R, Martínez-Navarrete G, Corrochano S, et al. Functional and structural modifications during retinal degeneration in the rd10 mouse. *Neuroscience*. 2008;155(3):698–713.
64. Phillips MJ, Otteson DC, Sherry DM. Progression of neuronal and synaptic remodeling in the rd10 mouse model of retinitis pigmentosa. *J Comp Neurol*. 2010;518(11):2071–2089.
65. Fernandez-Bueno I, Fernández-Sánchez L, Gayoso MJ, García-Gutierrez MT, Pastor JC, Cuenca N. Time course modifications in organotypic culture of human neuroretina. *Exp Eye Res*. 2012;104:26–38.
66. Fernández-Sánchez L, de Sevilla Müller LP, Brecha NC, Cuenca N. Loss of outer retinal neurons and circuitry alterations in the DBA/2J mouse. *Invest Ophthalmol Vis Sci*. 2014;55(9):6059–6072.
67. Hombrebueno JR, Chen M, Penalva RG, Xu H. Loss of synaptic connectivity, particularly in second order neurons is a key feature of diabetic retinal neuropathy in the Ins2Akita mouse. *PLoS One*. 2014;9(5):e97970.
68. Hombach S, Janssen-Bienhold U, Söhl G, et al. Functional expression of connexin57 in horizontal cells of the mouse retina. *Eur J Neurosci*. 2004;19(10):2633–2640.
69. Jin N, Zhang Z, Keung J, et al. Molecular and functional architecture of the mouse photoreceptor network. *Sci Adv*. 2020;6(28):eaba7232.
70. Feigenspan A, Janssen-Bienhold U, Hormuzdi S, et al. Expression of connexin36 in cone pedicles and OFF-cone bipolar cells of the mouse retina. *J Neurosci*. 2004;24(13):3325–3334.
71. Maxeiner S, Dedek K, Janssen-Bienhold U, et al. Deletion of connexin45 in mouse retinal neurons disrupts the rod/cone signaling pathway between AII amacrine and ON cone bipolar cells and leads to impaired visual transmission. *J Neurosci*. 2005;25(3):566–5676.
72. Dedek K, Schultz K, Pieper M, et al. Localization of heterotypic gap junctions composed of connexin45 and connexin36 in the rod pathway of the mouse retina. *Eur J Neurosci*. 2006;24(6):1675–1686.
73. Strettoi E, Raviola E, Dacheux RF. Synaptic connections of the narrow-field, bistratified rod amacrine cell (AII) in the rabbit retina. *J Comp Neurol*. 1992;325(2):152–168.
74. Veruki ML, Hartveit E. AII (Rod) amacrine cells form a network of electrically coupled interneurons in the mammalian retina. *Neuron*. 2002;33(6):935–946.
75. Bridge H, Plant GT. Conclusive evidence for human transneuronal retrograde degeneration in the visual system. *J Clin Exp Ophthalmol*. 2012;S3:1–4.
76. Dinkin M. Trans-synaptic retrograde degeneration in the human visual system: slow, silent, and real. *Curr Neurol Neurosci Rep*. 2017;17(2):16.
77. Park HY, Kim JH, Park CK. Alterations of the synapse of the inner retinal layers after chronic intraocular pressure elevation in glaucoma animal model. *Mol Brain*. 2014;7(1):1–11.
78. Weber AJ, Chen H, Hubbard WC, Kaufman PL. Experimental glaucoma and cell size, density, and number in the primate lateral geniculate nucleus. *Invest Ophthalmol Vis Sci*. 2000;41(6):1370–1379.
79. Yücel YH, Zhang Q, Weinreb RN, Kaufman PL, Gupta N. Effects of retinal ganglion cell loss on magno-, parvo-, koniocellular pathways in the lateral geniculate nucleus and visual cortex in glaucoma. *Prog Retin Eye Res*. 2003;22(4):465–481.
80. Wang R, Seifert P, Jakobs TC. Astrocytes in the optic nerve head of glaucomatous mice display a characteristic reactive phenotype. *Invest Ophthalmol Vis Sci*. 2017;58(2):924–932.


Investigative Ophthalmology & Visual Science

81. Sun D, Moore S, Jakobs TC. Optic nerve astrocyte reactivity protects function in experimental glaucoma and other nerve injuries. *J Exp Med*. 2017;214(5):1411–1430.
82. Bosco A, Breen KT, Anderson SR, Steele MR, Calkins DJ, Vetter ML. Glial coverage in the optic nerve expands in proportion to optic axon loss in chronic mouse glaucoma. *Exp Eye Res*. 2016;150:34–43.
83. Liddelow SA, Marsh SE, Stevens B. Microglia and astrocytes in disease: dynamic duo or partners in crime? *Trends Immunol*. 2020;41(9):820–835.
84. Almasieh M, Levin LA. Neuroprotection in glaucoma: animal models and clinical trials. *Annu Rev Vis Sci*. 2017;3:91–120.

Investigative Ophthalmology & Visual Science